Supplementary information on

Porous colloidal crystals in charged sphere suspensions by aggregate-driven phase separation

Nina Lorenz, Christopher Wittenberg, Thomas Palberg

Institute of Physics, Johannes Gutenberg Universität Mainz, Germany

1 Construction of dynamic maps

The transmission images on which we based the construction of the dynamic maps are rather featureless and do not allow for any discrimination of different phases. Aggregates are visible as tiny airy disks due to diffraction limited resolution. An example is shown in Fig. S1a. The corresponding dynamic map is shown in Fig. S1b.

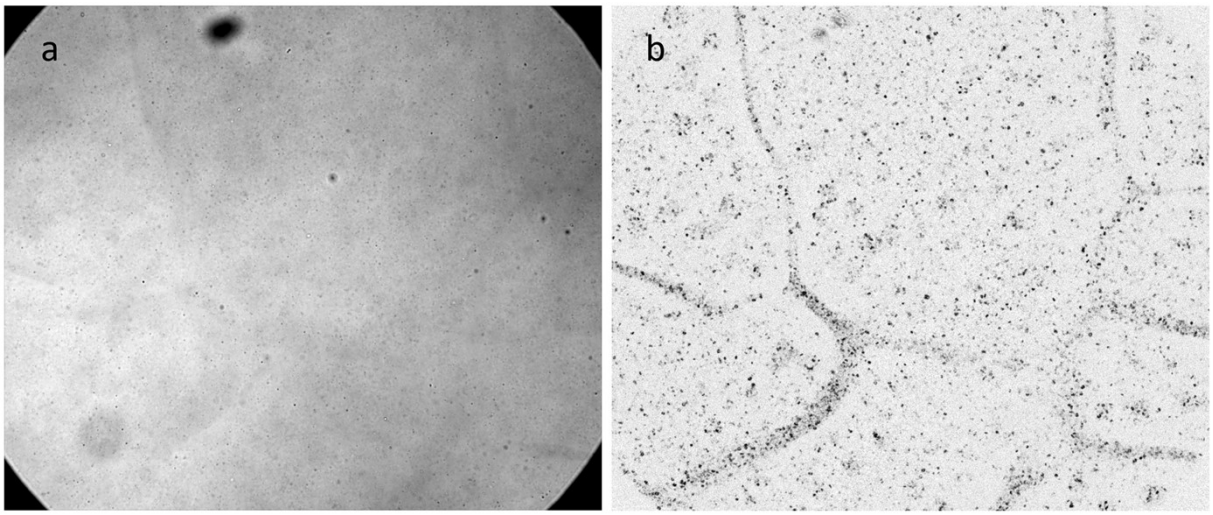

Figure S1. Construction of dynamic maps. a) B/w transmission image of a sample of aggregate-containing PnBAPS70 taken 24h after cell closing. **b)** corresponding dynamic map.

B/w Bragg microscopic images taken under oblique white light illumination allow discriminating different phases. Three examples taken 5d after cell closing in different regions of a sample of aggregate-containing PnBAPS70 are displayed in Fig. S2 a to c. They show crystals coexisting with a fluid phase. The corresponding dynamic maps are shown in Fig. S2d to e. Here we varied the lag time t' with respect to the fluid phase relaxation time $\tau_F \approx 3$ s ($\tau_S > 120$ s). In Fig. S2e, d and f, the lag times were $t' = 5$ s, $t' = 20$ s and $t' = 60$ s, respectively. A sufficient and reproducible discrimination between mobile and non-mobile regions was obtained for $\tau_S > t' >> \tau_F$.

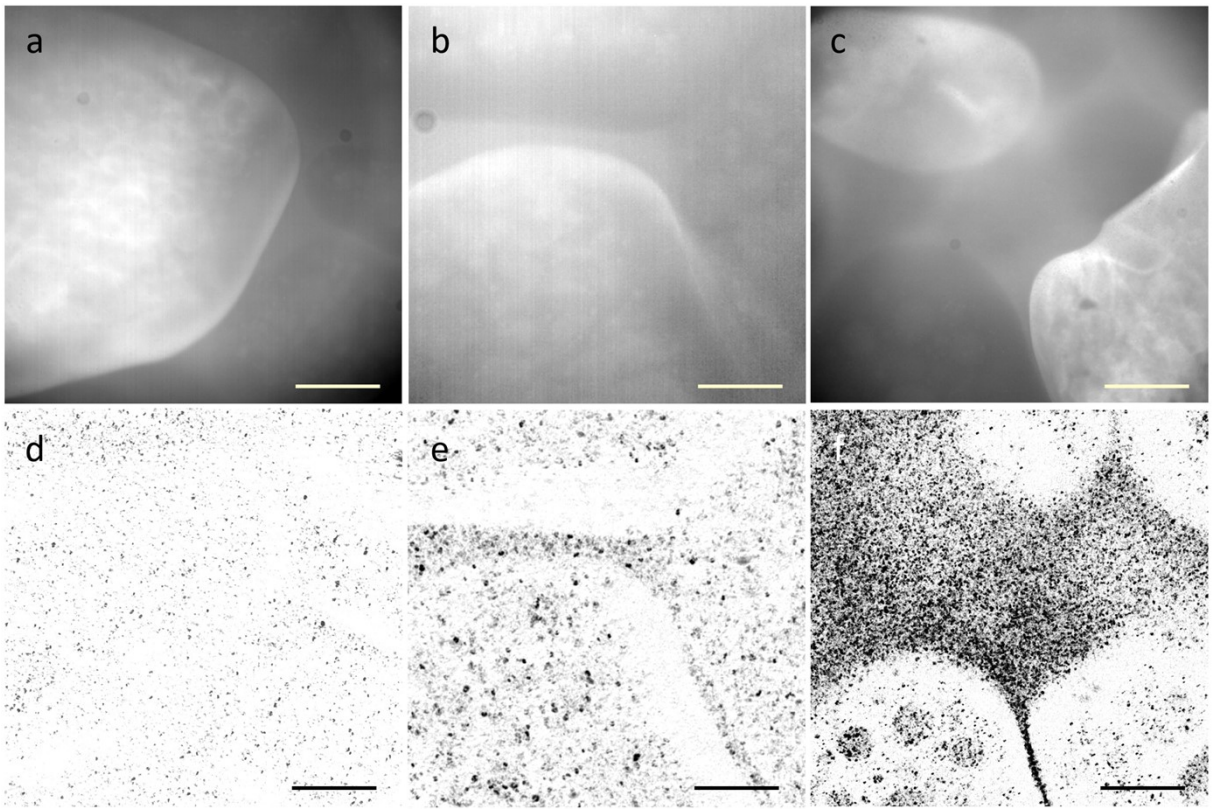

Figure S2. Variation of lag times. a) B/w Bragg microscopic images taken under oblique illumination 5d after cell closure in an aggregate containing suspension of PnBAPS70. Scal bar 200µm. **b)** The same but taken at another location within the sample. **c)** The same but taken at another location within the sample. **d)** Dynamic map constructed from transmission images taken at the location shown in (a) with lag time $t' = 5$ s. **e)** Dynamic map constructed from transmission images taken at the location shown in (b) with lag time $t' = 20$ s. **f)** Dynamic map constructed from transmission images taken at the location shown in (c) with lag time $t' = 60$ s. Only for sufficiently large lag times, a clear correlation between the location of crystallites, grain boundaries and other features found in the BM images and in the dynamic map is given.

2 Dynamic map of a stage I alloy formed in an aggregate-free binary mixture.

Aggregate-containing PnBAPS70 and binary mixtures of PnBAPS70 with PnBAPS122 are both two-component systems, but with significantly different particle size-ratios. It was therefore interesting to record the dynamic maps also for aggregate-free bulk samples of binary eutectic mixtures, conditioned by continuous cycling. Here, the only solid to appear is a polycrystalline substitutional alloy of bcc structure. The subsequent transformation stages seen in slit cells under slow deionization are all missing, Fig. S3a and b compares two dynamic maps taken on an aggregate-free, deionized sample at $n = 26\mu m^{-3}$ and $p_0 = 0.98$. Fig. S3a was taken 8h after cell closing and Fig. S3b 36h after cell closing. Initially, one observes activity concentrated in the vicinity of rather fuzzy grain boundaries. After extended times, the mobile regions have contracted to form irregularly shaped, but sharply bordered mobile pockets, distributed along the former grain boundaries. Neither mobile regions nor hole formation were observed inside aggregate-free alloy crystals.

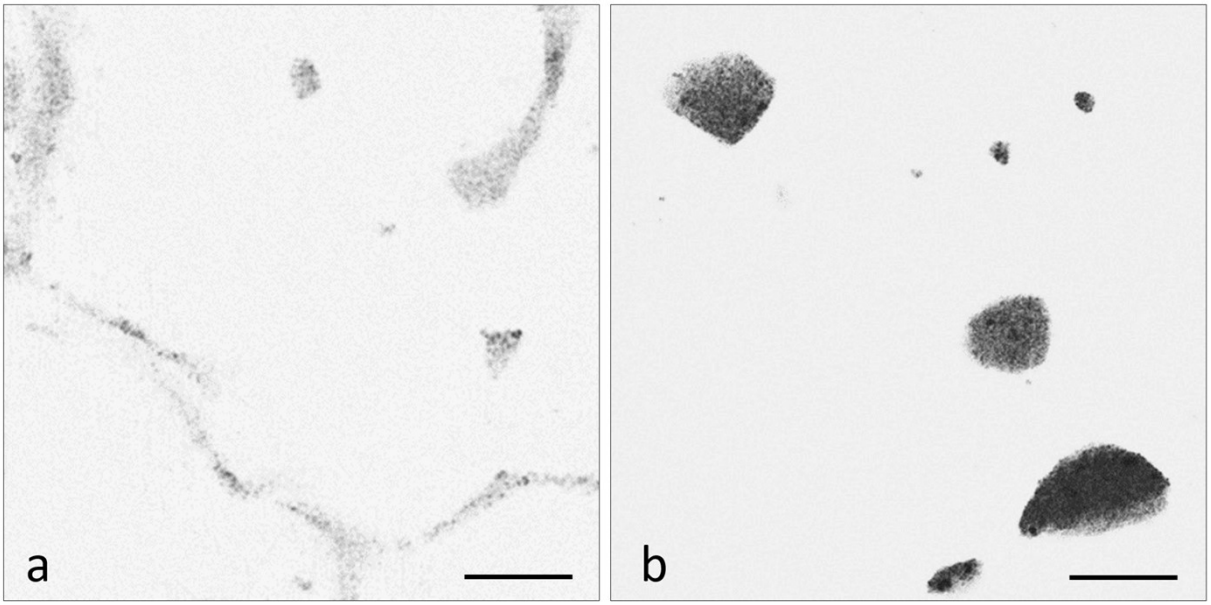

Figure S3. Dynamic map of a stage I alloy formed in an aggregate-free binary mixture. $n = 26\mu m^{-3}$ and $p_0 = 0.98$. Scale bars 200µm. **a)** Map taken 8 h after cell closure. **b)** Map taken 36 h after cell closure of a different region within the same sample.

3 Intermediate morphology of β-phase crystals in aggregate-containing binary mixtures.

Also β-phase crystals in aggregate-containing eutectic mixtures show holes. Rather large holes are present there from early on. This is illustrated in Fig. S4, featuring the central region of the slit cell observation chamber for a mixture at $p_0 = 0.94$ and $n = 38$ µm^{-3}. The image was taken 75 h after cell closure. Stage I alloys had initially formed closer to the reservoirs but already disappeared again. After 35 h, the β-phase appeared and grew vertically. Soon after, vividly coloured stage III crystals formed grew and shrunk again on top of the β-phase. Their secondary growth stage had not yet begun. The β-phase is here visible as a faint blueish background pattern. Both crystal types are seen to be perforated by holes, which are significantly larger and of more irregular shape within the β-phase. The scale bar is 250 µm.

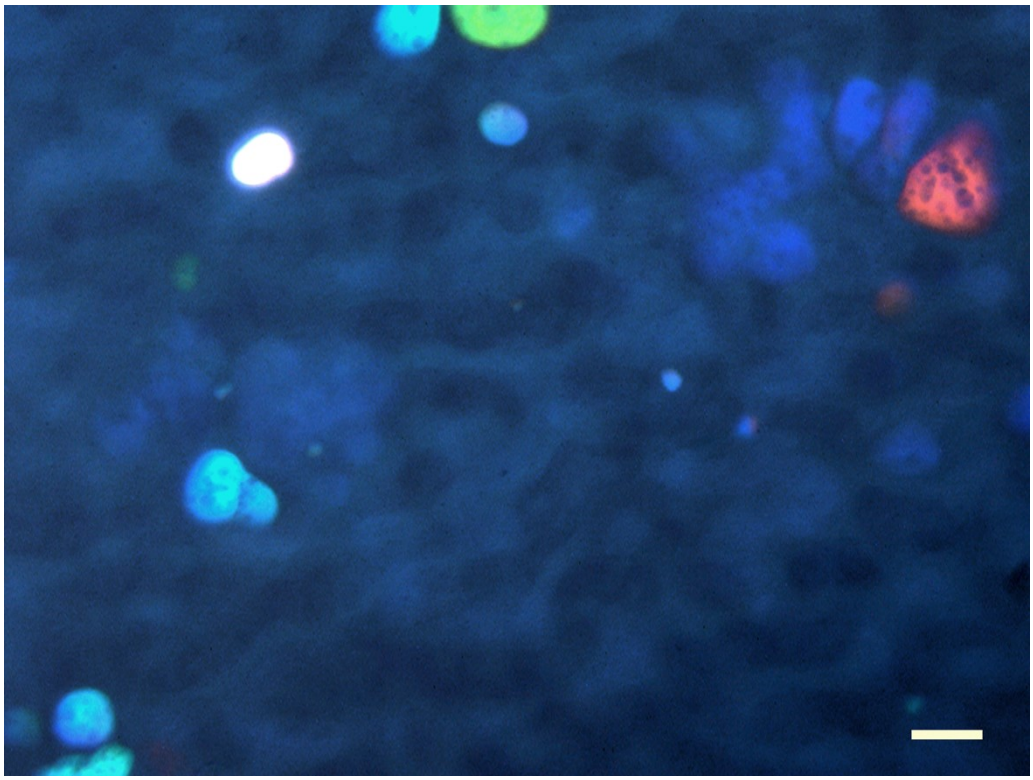

Figure S4. β-phase microstructure in an aggregate containing eutectic mixture. PM image taken in a slit cell at t = 75h after cell closure. $p_0 = 0.94$ and $n = 38$ µm^{-3}. Scale bar 250µm.

4 Additional data on aggregate free single component suspensions

In Fig. S5, we show exemplary micrographs of aggregate-free PnBAPS70 taken a few hours after solidification at $n = 24$ µm $^{-3}$ and $n = 15$ µm^{-3}. In both aggregate free samples, no holes are visible. Rather, in the Bragg micrograph of Fig. S5a, we see a mosaic of small, compact, intersection facetted crystals, typical for crystals grown after homogeneous bulk nucleation. In the PM micrograph Fig. S5b we see a close up of a crystallite intersections as observed for region of a larger wall nucleated crystals grown in columnar fashion.

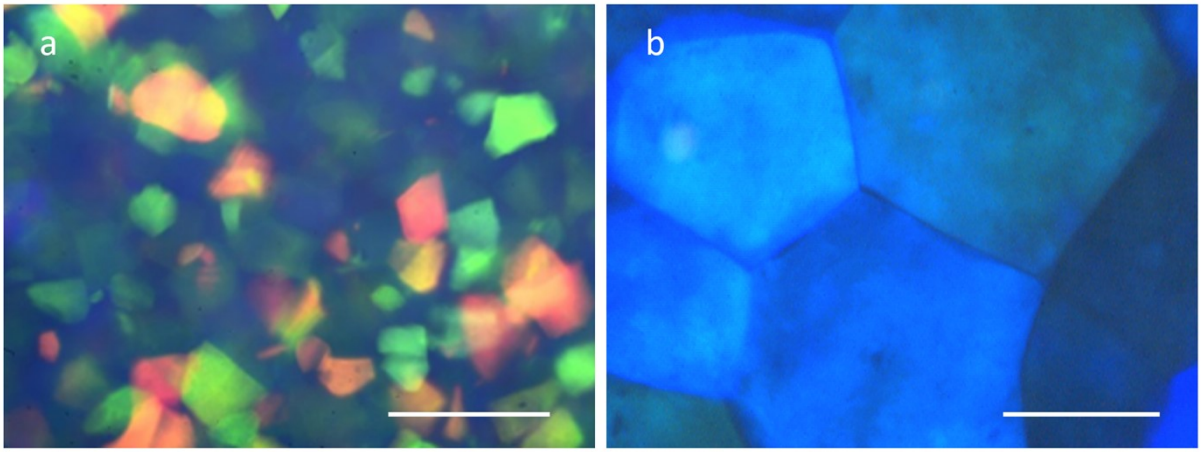

Figure S5: Crystals in aggregate free single component systems. a) PnBAPS70 at n = 13.5 µm^{-3}. Bragg micrograph. Scale bar 250µm. **b)** PnBAPS70 at n = 7.1 µm^{-3}. PM mode. Scale bar 100µm.

5 Additional data from static light scattering

For completeness we show in Fig. S6 a comparison of two samples of PNBAPS70 prepared under thoroughly deionized and decarbonized conditions by cycling them in gas-tight conditioning-circuit with integrated IEX-column. Sample cells were mounted in the index matching bath of a custom-built multi-purpose light scattering instrument [1], here run at a wave length of λ = 647.1 nm. Closing the samples off the circuit defined t = 0. The density was chosen low enough to avoid multiple scattering effects but large enough to ensure dominance of homogeneous bulk nucleation. With and without aggregates, both samples developed a polycrystalline microstructure via homogeneous nucleation and growth within some 20 minutes. First holes became discernible by visual inspection with a magnifying glass in the aggregate containing system after several hours. The light scattering data were taken after 4d with pores more clearly developed and visible also to the naked eye under suitable white light illumination.
We compare scattering data in terms of scattered intensity plotted versus scattering angle for an aggregate free sample (blue solid curve) and an aggregate-containing sample (black solid curve). Both samples show the typical peak shapes and sequence of Debye-Scherrer reflections for a bcc crystal structure [2]. The height of the main peak of the aggregate-containing sample is smaller and its full width at half height is somewhat larger due to a smaller extensions of compact crystallite regions. Overall, no significant differences in the peak shapes and positions are observed. Further, the total pore volume is too small, to show up in the development of a pronounced fluid peak. This is expectable. Additional scattering intensity should occur at small angles, which are sensible to variations in crystallite shape and further sensitive to the presence of aggregates. Angles below 20° are, however, not reliably accessed with the available machine. These should be addressed using small angle light scattering [3].

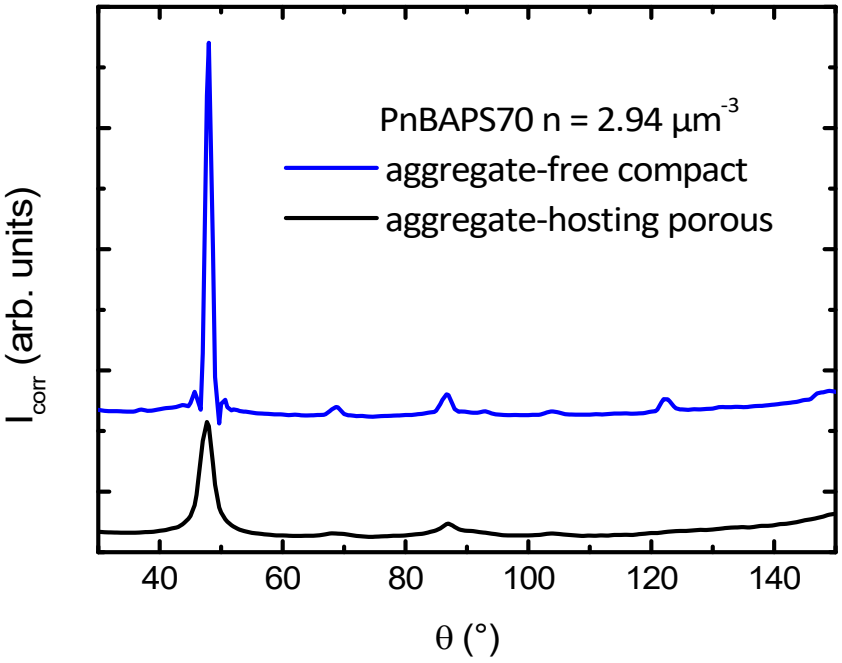

Figure S6: Static light scattering on crystallized PnBAPS70. Comparison of aggregate-free (blue) and aggregate-hosting (black) suspensions of same concentration. Presence of the seventh peak in the progression of Bragg reflections identifies the crystal structure as bcc for both samples. The difference between porous and compact microstructure is not reflected on the level of the interparticle distances.

---

[1] H.-J. Schöpe, T. Palberg, *J. Colloid Interface Sci.* **234**, 149-161 (2001). A multipurpose instrument to measure the vitreous properties of charged colloidal solids
[2] J. L. Langford, A. J. C. Wilson, *J. Appl. Cryst.* **11**, 102-113 (1978). Scherrer after Sixty Years: A Survey and Some New Results in the Determination of Crystal-lite Size
[3] R. Beyer, M. Franke, H. J. Schöpe, E. Bartsch and T. Palberg, *J. Chem. Phys.* **143**, 064903 (2015). From nuclei to micro-structure in colloidal crystallization: Investigating intermediate length scales by small angle laser light scattering